192   W. A. GOBIE, C. F. IVORY

Fig. 1. Taylor dispersion in a heated capillary. The temperature profile in the lumen distorts the sample's electrophoretic velocity. Molecular diffusion ameliorates the effect by radially averaging the concentration. The sample is depicted migrating opposite the direction of electroosmotic flow. t = time.

a constant-voltage mode, the current will increase, thereby increasing the power dissipated in the buffer and warming the buffer further. The apparatus always runs hotter than a constant-conductivity model would predict. Further, there is a critical voltage above which a temperature increase produces a greater increase in Joule heating than in heat transfer to the coolant. Under such conditions the device experiences "autothermal runaway". This phenomenon places an absolute limit on the voltage which may be used, and is not predicted by a constant conductivity model.

Grushka et al.[3] omitted the autothermal effect on the grounds that the difference between the autothermal and constant-conductivity temperature profiles is rather small in CE[5] and does not justify the additional mathematical complexity. This is often the case. But since one of our purposes here is to examine modifications to CE which will permit operation with significant temperature gradients, we shall employ the more rigorous model.

Since thermal Taylor dispersion is due to a nearly parabolic variation in electrophoretic velocity, we realized that it might be possible to compensate for the variation by opposing it with a small Poiseuille flow, as depicted in Fig. 2. Hertén[6] has used a Poiseuille flow to compensate for electroosmotic dispersion in closed-end tubes, where the goal was to flatten the hydrodynamic velocity profile by opposing a laminar flow with a second laminar flow. Our object is to distort the hydrodynamic flow in the capillary to compensate for the thermally induced distortion of the sample's velocity.

The band broadening model we present incorporates a laminar flow as well as our autothermal thermal model. We find that a small Poiseuille flow can dramatically improve column performance, although such improvement may be chimerical unless one can reduce the initial length of the sample to 1 mm or less. Our proposed method seems to hold the most promise for very large capillaries, i.e. those with internal
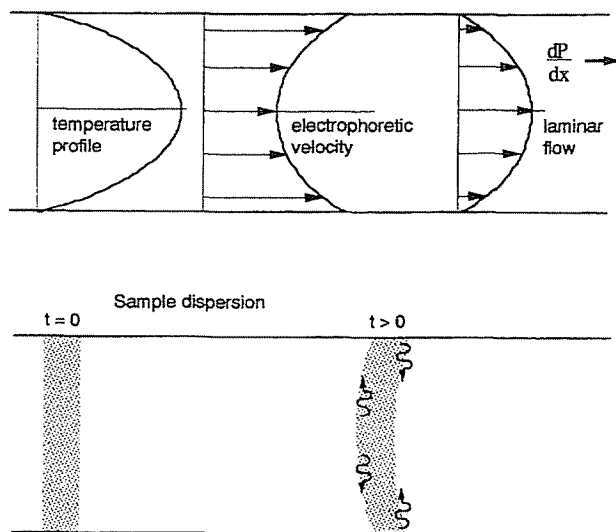
A 15

THERMAL MODEL OF CE

Fig. 2. By opposing the distortion of the sample's electrophoretic velocity with a laminar flow, it is possible to give the sample a nearly flat velocity profile.

diameters of 400 μm or more, for which it appears possible to obtain plate numbers of 10^6 m^{-1} or more. The ability to use such large capillaries could considerably ease detection problems; for the same sample length, sample loading in a 500-μm capillary is 100 times greater than in a 50-μm I.D. capillary.

THEORY

Thermal model

    The theory of electrically heated cylindrical objects is well established (*e.g.*, see ref. 7). Hinkley[8], and Coxon and Binder[9] gave the first analyses specific to tubular electrophoresis equipment. Grushka *et al.*[3] and Jones and Grushka[5] have recently presented analyses specifically for CE. Our analysis considers in greater detail (i) the ramifications of the autothermal effect and (ii) the sensitivity of the capillary to heat transfer conditions.
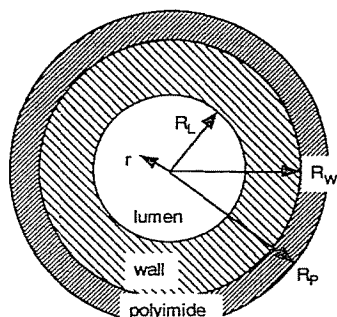

Fig. 3. Capillary cross section, showing the lumen, silica wall and polyimide coat.

A 16

Fig. 3. shows the geometry used for the capillary. The energy balance on the buffer in the lumen is

$$k \frac{1}{r} \frac{\mathrm{d}}{\mathrm{d}r} r \frac{\mathrm{d}T}{\mathrm{d}r} = -E^2 \kappa \tag{1}$$

Here r is the radial coordinate, T the buffer temperature, E the electric field, k the thermal conductivity of the buffer and κ the electrical conducivity.

At the centerline the temperature must be finite. Heat transfer from the capillary surface to the surroundings is described by an overall heat transfer coeffient h_{OA}. The boundary conditions are accordingly

$$-k \frac{\mathrm{d}T}{\mathrm{d}r} = \begin{array}{ll} T \text{ finite} & r = 0 \\ h_{OA}(T - T_C) & r = R_L \end{array} \tag{2}$$

In the second boundary condition T_C is the coolant temperature. The heat transfer coefficient is obtained by combining the thermal resistances of the silica wall, the polyimide coat, and the surface resistance according to the usual rule for cylindrical geometry[7]:

$$h_{OA} = \frac{1}{R_L} \frac{1}{\dfrac{\ln \dfrac{R_W}{R_L}}{k_w} + \dfrac{\ln \dfrac{R_P}{R_W}}{k_p} + \dfrac{1}{R_p h_s}} \tag{3}$$

The radii R_W, R_L and R_p are as shown in Fig. 3, k_w and k_p are the thermal conductivity of the wall and polyimide coat, and h_s is the surface heat transfer coefficient. For a liquid-cooled capillary, h_s will be so large that its term in eqn. 3 can be neglected. For an air-cooled capillary, h_s is a function of the surface temperature T_S, which can be found by equating the rates of heat transfer at the lumen surface and the outer capillary surface:

$$-R_L k \frac{\mathrm{d}T}{\mathrm{d}r} \bigg|_{r=R_L} = R_P h_S(T_S - T_C) \tag{4}$$

As detailed below, h_S can be calculated from a correlation involving a low-order non-linearity in T_S.

A linear model of the electrical conducitivity is mathematically convenient and is usually a good approximation over a 10–20°C temperature range:

$$\kappa = \kappa_0 [1 + \kappa_1 (T - T_0)] \tag{5}$$

Here T_0 is a reference temperature, κ_0 the conductivity at T_0, and κ_1 the temperature coefficient. For mathematical convenience we will take $T_0 = T_C$ with no loss of generality.

Using the dimensionless variables defined in Table I puts the model in the form

A 17

THERMAL MODEL OF CE   195

TABLE I

DIMENSIONLESS VARIABLES

$\theta = \dfrac{T - T_0}{\Delta T_{\text{ref}}}$	Dimensionless temperature
$\eta = r/R_{\text{L}}$	Dimensionless radial coordinate
$\Delta T_{\text{ref}} = \dfrac{\kappa_0 E^2 R_{\text{L}}^2}{k}$	Characteristic temperature rise
$\lambda = \sqrt{\kappa_1 \Delta T_{\text{ref}}}$	Autothermal parameter
$Bi_{\text{OA}} = \dfrac{h_{\text{OA}} R_{\text{L}}}{k}$	Overall Biot number

$$\frac{1}{\eta}\frac{\mathrm{d}}{\mathrm{d}\eta}\,\eta\,\frac{\mathrm{d}\theta}{\mathrm{d}\eta} + \lambda^2\theta = -1$$

$$\tag{6}$$

$$-\frac{\mathrm{d}\theta}{\mathrm{d}\eta} = \begin{matrix} \theta \text{ finite} \\ \tfrac{1}{2} Bi_{\text{OA}}\theta \end{matrix} \qquad \begin{matrix} \eta = 0 \\ \eta = 1 \end{matrix}$$

Here k is the "autothermal parameter", the characteristic increase in electrical conductivity due to the characteristic temperature rise ΔT_{ref}. Bi_{OA} is the overall Biot number, a dimensionless heat transfer coefficient which compares the rate of heat conduction through the composite wall with the rate at which heat is removed by the coolant.

The scaled surface temperature θ_{S} is found from scaling eqn. 4

$$-\frac{\mathrm{d}\theta}{\mathrm{d}\eta}\Bigg|_{\eta=1} = \frac{1}{2}\,Bi_{\text{S}}\theta_{\text{S}}$$

$$\tag{7}$$

where Bi_{S} is the surface Biot number, $h_{\text{S}}R_{\text{P}}/k$.

The dimensionless temperature inside the capillary is found to be

$$\theta = \frac{1}{\lambda^2}\,\frac{J_0(\lambda\eta) - J_0(\lambda) + \dfrac{2\lambda}{Bi_{\text{OA}}}\,J_1(\lambda)}{\mathrm{f}(\lambda)}$$

$$\tag{8}$$

J_0 and J_1 are Bessel functions of the first kind. The first two terms in the numerator give the temperature variation across the lumen radius, while the last term gives the temperature at the lumen surface. The function $\mathrm{f}(\lambda)$ expresses the autothermal effect, $i.e.$, the additional temperature rise due to the feedback between temperature and power density. It is given by

$$\mathrm{f}(\lambda) = J_0(\lambda) - \frac{2\lambda}{Bi_{\text{OA}}}\,J_1(\lambda)$$

$$\tag{9}$$

A 18

For non-zero λ, $f(\lambda)$ is always less than unity, so the capillary always runs hotter than would be predicted by a constant-conductivity model. Further, at a crital value of the autothermal parameter, λ^*, $f(\lambda^*)$ vanishes, implying *autothermal runaway*. Under such conditions the capillary is unable to attain thermal equilibrium by increasing its temperature, and the temperature rises until a vapor bubble forms. The threshold for autothermal runaway establishes an absolute upper bound on the voltage one may apply. In practice the buffer usually boils before λ^* is reached.

The largest critical value of the autothermal parameter is obtained with perfect cooling, *e.g.*, by forced liquid cooling of a capillary with a vanishingly thin wall. Setting the overall Biot number Bi_{OA} to infinity in eqn. 9 shows that the maximum critical value is $\lambda^* \approx 2.4$, the first root of J_0.

In general, the heat transfer resistance is quite significant. Fig. 4 shows how the overall Biot number depends on the temperature difference between the surface of the capillary and the surroundings for a 100×200 (I.D. $\times$ O.D.) μm capilary cooled by natural convection in air. The method of calculation is described below. A typical value of Bi_{OA} for rough calculations can be taken as 0.055. For the same capillary with forced liquid cooling, the surface resistance can be neglected, giving a Bi_{OA} value of about 1.2. A similar result can be obtained with vigorous forced air cooling.

For $Bi_{OA} \leqslant 5$, $f(\lambda)$ can be well approximated by replacing the Bessel functions in eqn. 9 with the leading terms of their power series through $O(\lambda^4)$:

$$f(\lambda) = \frac{1}{8}\left[\frac{1}{Bi_{OA}} + \frac{1}{8}\right]\lambda^4 - \left[\frac{1}{Bi_{OA}} + \frac{1}{4}\right]\lambda^2 + 1 \qquad (10)$$

From this one can obtain

$$\lambda^* = \sqrt{\frac{1}{\dfrac{1}{Bi_{OA}} + \dfrac{1}{8}}} \qquad (11)$$

For natural convection air-cooled capillaries this expression shows that $\lambda^* \approx \sqrt{Bi_{OA}}$. The relative inefficiency of air cooling compared to liquid cooling can be gauged by using the rough values for Bi_{OA} of 0.055 and 1.2 in eqn. 11. Ignoring the question of when the buffer will boil, a factor of $\lambda^*_{\text{liquid}}/\lambda^*_{\text{air}} \approx 18$ times greater voltage can be applied to a 100×200 μm·capillary if it is liquid cooled.
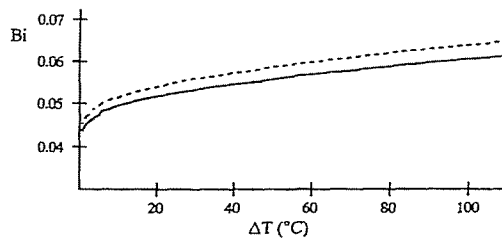

Fig. 4. Biot number for a 100×200 μm air-cooled capillary as function of temperature difference between the surface and surroundings. Solid line is overall Biot number, dashed line is surface Biot number. Surface resistance dominates heat transfer for air cooled capillaries.

For natural convection air-cooled capillaries the small magnitude of λ permits us to replace the Bessel functions in eqn. 8 with the first few terms of their power series, giving

$$\theta \approx \frac{\dfrac{1}{4}(1 - \eta^2) + \dfrac{\lambda^2}{64}(\eta^4 - 1) + \dfrac{1}{Bi_{OA}}\left(1 - \dfrac{\lambda^2}{8}\right)}{f(\lambda)} \tag{12}$$

Taking the limit $\lambda \to 0$ in eqn. 12 while holding Bi_{OA} constant in $f(\lambda)$ gives the parabolic temperature profile of refs. 3 and 5. But since the critical value λ^* for air-cooled capillaries is quite small, the value of λ in practice will generally be an appreciable fraction of λ^*. Thus $f(\lambda)$ will be small and the autothermal effect pronounced. Therefore, while the temperature profiles obtained in refs. 3 and 5 give the correct shape, they may seriously underpredict the magnitude of the temperature variation.

Heat transfer coefficient

For capillaries cooled by forced convection of air or liquid, the surface heat transfer coefficient will generally be so large that the surface resistance will be negligible in eqn. 3. Cooling by natural convection in air is much less efficient, so the surface resistance cannot be neglected.

Heat transfer coefficient for natural convection air cooling

The surface resistance is the most significant resistance to heat transfer for a natural convection air-cooled capillary, although at higher temperatures radiation can account for 10–20% of the heat loss. If the capillary is shielded from drafts, the convective contribution can be calculated from standard correlations for natural convection from a horizontal cylinder. For the calculations reported here, we used the following slightly modified form of McAdams'[10] correlation for the convective Nusselt number:

$$Nu_C = 0.45 + 0.55\,(GrPr)^{\frac{1}{4}} \tag{13}$$

The modification consisted of adding the asymptotic value 0.45 and adjusting the multiplicative constant to improve the fit to McAdams' recommended interpolation points. Gr and Pr are the Grashof and Prantl numbers.

The radiant heat transfer coefficient is calculated assuming equal emissivities for the polyimide and surroundings:

$$Nu_r = \frac{2R_P}{k_c}\,\frac{\sigma e(T_S^4 - T_C^4)}{T_S - T_C} \tag{14}$$

Here e is the emissivity, σ is the Stefan-Boltzmann constant, and k_C is the thermal conductivity of the coolant (air). A surface Nusselt number is obtained by adding the convective and radiative Nusselt numbers, $Nu_S = Nu_C + Nu_R$, and Nu_S is converted to a surface Biot number by

$$Bi_S = \frac{k_C}{k}\frac{R_P}{R_L}Nu_S \qquad (15)$$

Since the heat transfer coefficients and surface temperature are coupled non-linearly, iteration is required to determine the capillary temperature. However, the radiative component is relatively small, and the non-linearity of the convective component is low-order, so the calculation is not a difficult one.

Band spreading model

Band spreading in CE can be treated as a problem in Taylor dispersion[2], in which radial diffusion tends to average out radial concentration variations produced by convective dispersion. Whether such treatment is accurate depends upon the capillary dimensions and the substances being analysed. Gill and Sankarasubramanian[11] have shown that the residence time L/U must satisfy

$$\frac{L}{U} \gg 0.5\frac{R_L^2}{D} \qquad (16)$$

This criterion is easily satisfied for capillaries up to 100 μm inner radius and proteins with diffusion coefficients of $O(10^{-6}$ cm^2/s). For significantly larger capillaries the analysis looses rigor, because the residence time is not long enough to allow thorough radial mixing by diffusion. However, the result remains adequate for the purposes of gauging the effectiveness of adding a Poiseuille flow and of estimating the required magnitude of the flow.

Aris'[12] formulation is the appropriate starting point. The mean velocity of a tracer pulse is given by

$$U = 2\int_0^1 u\eta\,d\eta \qquad (17)$$

Here u is the sample's velocity. It is determined by the material's electrophoretic mobility α, the electroosmotic mobility α', and the Poiseuille flow. Each of these velocities depends on temperature through the variation of viscosity with temperature. In the most general form, the velocity is

$$u = E\alpha' + E\alpha - \frac{R_L^2}{4\mu}\frac{dP}{dx}(1 - \eta^2) \qquad (18)$$

The rate at which the pulse spreads is characterized by the rate of growth of its second moment, given by[12]

$$\frac{dm_2}{dt} = 2 + 4\frac{R_L}{D}\int_0^1 \eta c_1\chi\,d\eta \qquad (19)$$

where χ is the departure from the mean velocity[12]

$$\chi = u - U \qquad (20)$$

A 21

THERMAL MODEL OF CE   199

and c_1 is the radial variation from the mean concentration[12]

$$c_1 = -\frac{R_L}{D}\int_0^\eta\int_0^{\eta'}\chi\eta\,d\eta\frac{1}{\eta'}\,d\eta' \tag{21}$$

From the second moment we obtain the effective, or Taylor, diffusion coefficient[12]:

$$D_T = \frac{1}{2}\frac{dm_2}{dt} \tag{22}$$

Evaluating eqns. 19 and 21 using the temperature profile of eqn. 8 and an exact formula for the viscosity[13] is best done numerically. However, for air cooled capillaries, we can use the approximate temperature profile, eqn. 11, and express the temperature dependence of viscosity with the following linear perturbation:

$$\frac{1}{\mu} = \mu_0[1 + \omega^2\theta\,(\eta)]$$
$$\omega = \sqrt{\mu_1\Delta T_{ref}} \tag{23}$$

Here μ_0 is the reciprocal viscosity at T_0, and μ_1 is the temperature coefficient. The integrands in eqns. 17, 19 and 21 are then polynomials, and after some tedium one finds

$$U = \left(-\frac{1}{8}R_L^2\,\mu_0\frac{dP}{dx}\right)\left[\frac{\left(\frac{1}{Bi_{OA}}+\frac{1}{6}\right)\omega^2}{f(\lambda)}+1\right]+$$
$$+\left[\left(\frac{\lambda^2}{Bi_{OA}f(\lambda)}+1\right)(\alpha_0+\alpha_0')+\frac{1}{8}\frac{\alpha_0\lambda^2}{f(\lambda)}\right]E \tag{24}$$

$$D_T = D\left\{1+\frac{1}{3072}\frac{R_L^2}{D^2}\left[\left(\frac{\omega^2}{Bi_{OA}f(\lambda)}+1\right)R_L^2\mu_0\frac{dP}{dx}-\frac{E\alpha_0\lambda^2}{f(\lambda)}\right]^2\right\} \tag{25}$$

Only the dominant terms for small Bi_{OA}, λ and ω have been retained in these expressions. The factor enclosed in square brackets (eqn. 25) is the mean value of the velocity distortion. Here we see the desired effect: dP/dx can be adjusted to reduce the effective dispersion coefficient to the diffusive limit. We find

$$\frac{dP}{dx} = \frac{E\alpha_0\lambda^2}{\left[\frac{\omega^2}{Bi_{OA}f(\lambda)}+1\right]R_L^2\mu_0f(\lambda)} \tag{26}$$

In using this equation it must be borne in mind that the mobility α_0 and electric field E are signed quantities. Because the pressure gradient affects the mean velocity,

A 22

eqn. 26 may not maximize the plate number. We investigate this question after defining the plate number.

The plate number is usually defined as

$$N = \frac{UL}{2D_T} \tag{27}$$

Eqn. 27 does not necessarily predict the plate numbers that would be deduced in practice from measurements of output peak widths. This because the increase in peak width may be so small in CE that the output peak width is substantially determined by the initial size of the sample. This effect can be quantified by adding the initial variance of the sample to the increase in variance produced in the column go give the "observed" plate number:

$$N_{obs} = \frac{1}{2\dfrac{D_T}{LU} + \dfrac{1}{12}\dfrac{z^2}{L^2}} \tag{28}$$

Here z is the initial length of the sample.

We can estimate the optimal pressure gradient by substituting eqns. 24 and 25 into eqn. 27, differentiating with respect to dP/dx, and setting the result to zero. A quadratic equation in dP/dx is obtained. One root is rejected since it leads to a negative value for N. The remaining root is quite complicated; for clarity we retain temperature dependence only in the terms involving the mobility of the sample:

$$\frac{dP}{dx} = 8\,\frac{(\alpha_0 + \alpha'_0)E}{R_L^2\mu_0}$$

$$- \sqrt{3072\,\frac{D^2}{R_L^6\mu_0^2} + \frac{E^2}{R_L^4\mu_0^2}\left[-8(\alpha_0 + \alpha'_0) + \frac{\alpha_0\lambda^2}{f(\lambda)}\right]^2} \tag{29}$$

The first term under the root and the second term inside the square brackets are generally much smaller than the first term inside the brackets. Using the Taylor series approximation

$$a - \sqrt{c + (-a+b)^2} \approx b - \frac{1}{2}\frac{c}{a} \tag{30}$$

where $|a| >> \{|b|, |c|\}$, we can estimate

$$\frac{dP}{dx} \approx -192\,\frac{D^2}{(\alpha_0 + \alpha'_0)ER_L^4\mu_0} + \frac{E\alpha_0\lambda^2}{R_L^2 f(\lambda)\mu_0} \tag{31}$$

The first term is generally much smaller than the second, so we conclude that pressure gradients which minimize the effective dispersion coefficient little affect the mean velocity. Eqn. 26 adequately estimates the optimal pressure gradient.

A 23

EXPERIMENTAL

We used four untreated silica capillaries, donated by Polymicro Technologies. The capillary dimensions are given in Table II. The actual diameters of the ends of the capillaries were measured under a microscope. The power supply was a Spellman UHR-30, with a maximum output of 30 kV. Voltage was read from the power supply's front panel meter and current from a Hewlett-Packard 412A multimeter connected in series on the grounded side of the capillary.

The buffer used for all the experiments contained 10 mM sodium phosphate, adjusted to pH 7.0 by mixing 10 mM monobasic sodium phosphate and 10 mM dibasic sodium phosphate, and 50 mM KCl. The buffer was degassed immediately before experiments by agitating it while under a 600 mmHg vacuum. Upon heating, the degassed buffer began to outgas at 80–85°C.

The sodium phosphate–KCl buffer's conductivity has the desirable property of virtually linear variation with temperature, as shown in Fig. 5. The buffer conductivity was measured with a YSI Model 35 conductance meter and YSI 3417 conductivity cell.

In use, a capillary was positioned nearly horizontally, with its ends dipping into 50-ml beakers which served as buffer reservoirs. The capillary, supports, and beakers were enclosed in a plexiglass box 91 cm wide, 50 cm deep and 107 cm high (36 × 20 × 42 in.). The door of the box actuated interlock switches, which disabled the power supply when the door was open. In addition to providing operator safety, the box shielded the capillary from strong drafts.

An experiment consisted of measuring the current passed by the capillary at fixed voltages, and terminated when a vapor bubble formed in the capillary. Average temperature in the lumen was then inferred from the calibration shown in Fig. 5.

RESULTS

Temperature experiments and thermal model

Figs. 6–9 show comparisons of experiment and theory. The curves labeled "Autothermal theory" give the predicted average temperature obtained by radially averaging eqn. 10. The curves labeled "$\lambda = 0$" show the temperatures predicted by a constant-conductivity model. The actual capillary dimensions given in Table II were used in the calculations. The heat transfer coefficient was calculated using eqns. 13–15.

For reasons discussed below, the autothermal model generally overpredicts the

TABLE II

CAPILLARY DIMENSIONS

Nominal dimensions (µm, I.D. × O.D.)	Actual lumen diameter (µm)	Actual wall diameter (µm)	Actual polyimide thickness (µm)	Length (cm)
250 × 350	263	313	21	91.7
250 × 530	257	510	15	101.2
100 × 200	98	172	18	100.3
75 × 150	78	133	8.5	146.8

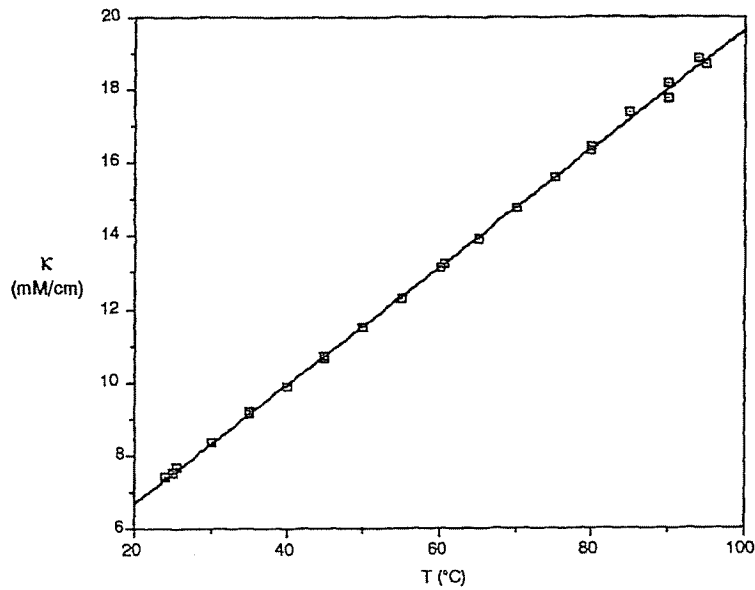**A 24**

W. A. GOBIE, C. F. IVORY

Fig. 5. Conductivity of the sodium phosphate–potassium chloride buffer used in the temperature experiments.
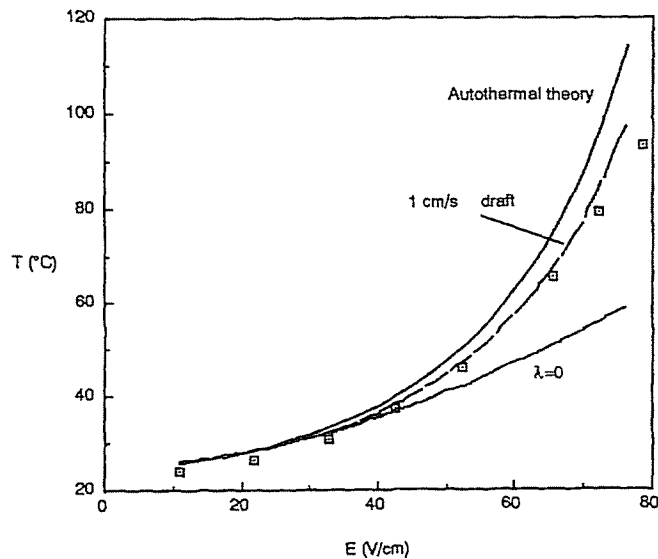
Fig. 6. Comparison of experimentally measured capillary temperature and theory for the 250 × 350 μm capillary. This figure also shows the effect of a 1-cm/s draft on the predicted capillary temperature.

A 25

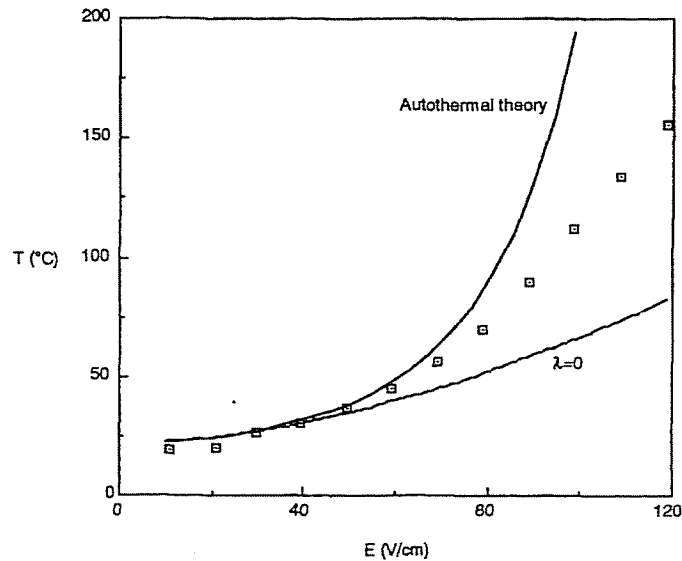THERMAL MODEL OF CE   203

Fig. 7. Comparison of experimentally measured temperature and theory for the 250×530 μm capillary. This capillary exhibited about 50°C superheating.

capillary temperature, while the constant-conductivity model underpredicts it. At higher voltages the discrepancy between the data and constant-conductivity model approaches 40°C.

The discrepancy between our data and the predictions of the autothermal model is most likely due to slow circulation of air inside the apparatus enclosure. We explored
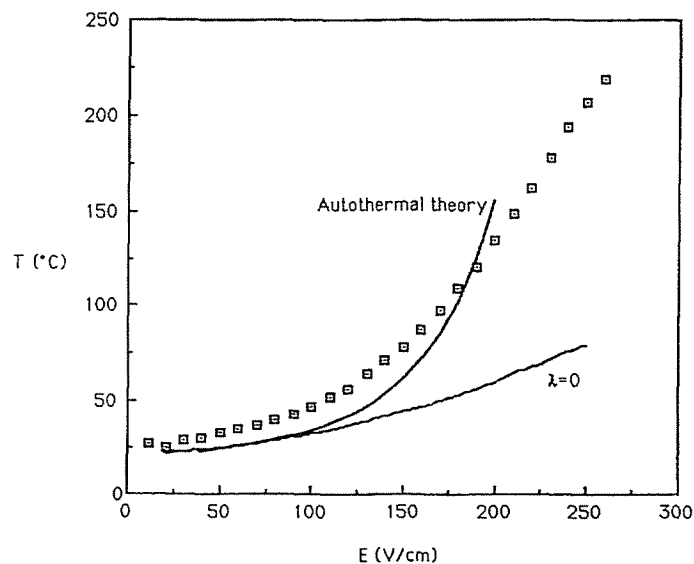

Fig. 8. Comparison of experimentally measured temperature and theory for the 100×200 μm capillary. This capillary exhibited more than 100°C superheating.

A 26

W. A. GOBIE, C. F. IVORY

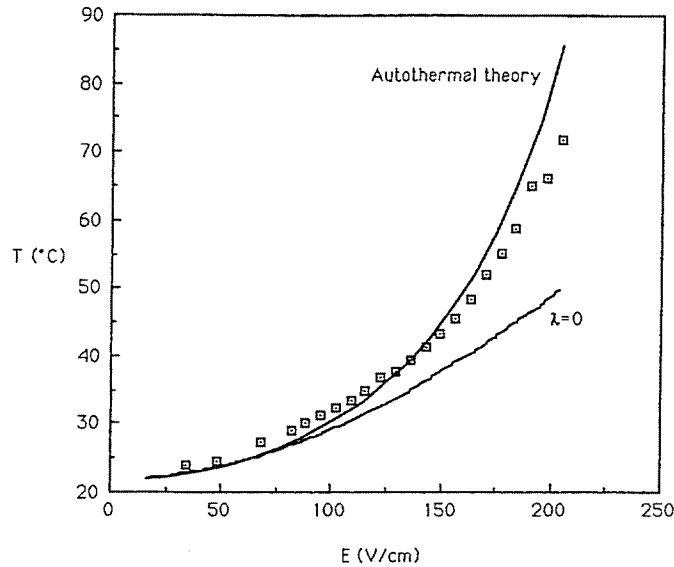Fig. 9. Comparison of experimentally measured temperature and theory for the 75 × 150 μm capillary.

this effect by incorporating a 1 cm/s draft into the surface heat transfer coefficient used for the 250 × 350 μm capillary simulation. As shown in Fig. 6, this markedly improves the agreement with experiment. Because convection reduces the capillary temperature, adding a draft to the constant-conductivity simulations would only worsen the predictions of the constant-conductivity model.

A remarkable feature of Figs. 7 and 8 is the superheated temperatures achieved in these capillaries, some 50 and 120°C above the boiling point. A direct measurement of the temperature was made for the 100 × 200 capillary: a thermocouple, approximately 1 mm in diameter, was placed in contact with the capillary near the grounded end. Thermal contact was improved with a small amount of Omegatherm 201 thermally conductive paste (Omega Engineering). Although this arrangement gave only a crude measurement of the surface temperature, the thermocouple registered 107°C at the highest electric field, verifying the occurrence of superheating.

TABLE III

PARAMETERS USED FOR PLATE NUMBER SIMULATIONS

$\alpha_0 = 4$ μm cm/V s
$\alpha'_0 = 8$ μm cm/V s
$D = 1 \cdot 10^{-6}$ cm^2/s
$k = 6$ mW/cm °C
$\kappa_0 = 10$ mS/cm
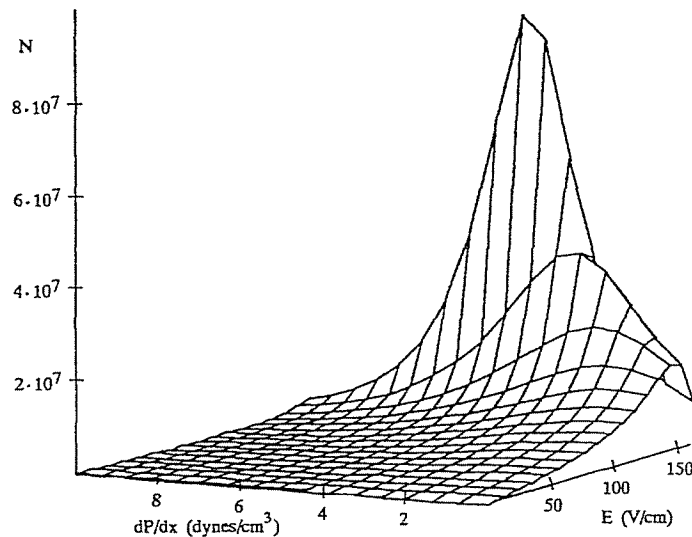$\kappa_1 = 0.046$ °C^{-1}
$\mu_0 = 100$ cm s/g
$\mu_1 = 0.011$ °C^{-1}

Fig. 10. Plate number for an air-cooled, 100 cm long, 100 × 200 μm capillary. By applying a pressure gradient it is possible to increase N by as much as 10 times.

Dispersion model

Parameters used for the following calculations are given in Table III. Fig. 10 shows the plate number predicted for an air cooled, 100 cm long, 100 × 200 μm capillary as a function of pressure gradient and electric field. With no pressure gradient, this capillary can achieve approximately 10^6 plates. When a pressure gradient is applied the plate number can be doubled at 150 V/cm, and increased to about 10^7 plates at higher voltages. The pressures required are modest: 5 dynes/cm² cm over
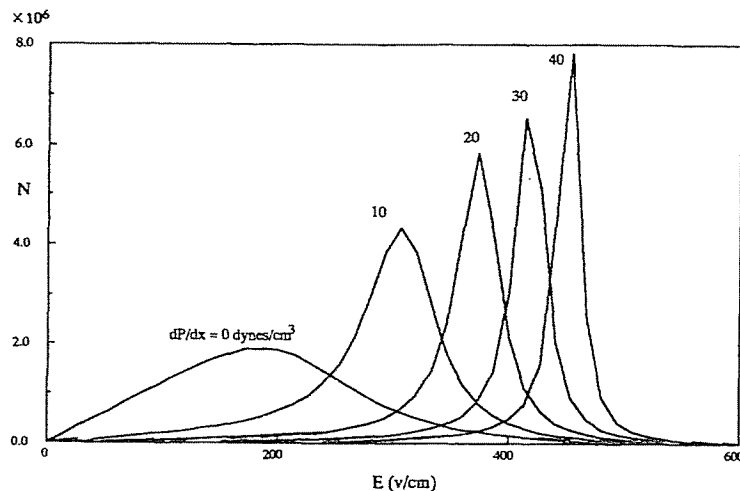

Fig. 11. Plate number for a liquid-cooled, 20 cm long, 100 × 200 μm capillary as a function of electric field for various applied pressure gradients.

A 28

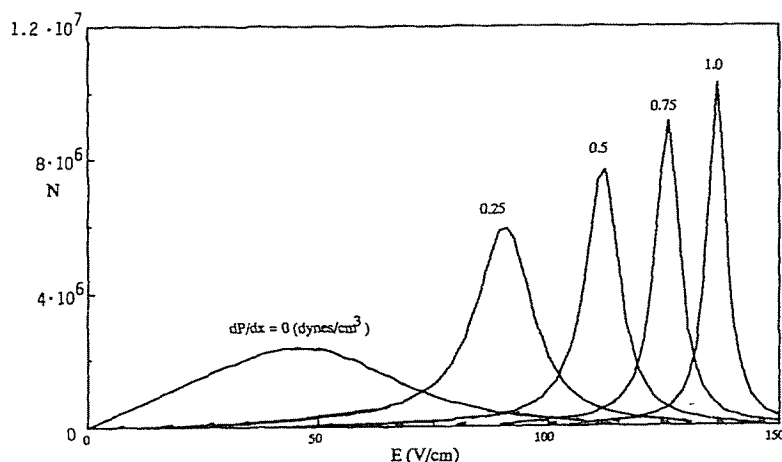206   W. A. GOBIE, C. F. IVORY

Fig. 12. Plate number for a liquid-cooled, 100 cm long, 400 × 530 μm capillary. Remarkably high plate numbers can be obtained despite the large inner diameter.

a 100 cm capillary is equivalent to a difference in elevation of the buffer reservoirs of about 5 mm.

Fig. 11 shows the plate number predicted for a liquid cooled, 20 cm long, 100 × 200 μm capillary. This capillary can also approach 10^7 plates when a pressure gradient is applied. Higher pressure gradients are required here than for the air cooled case because the temperature variation across the lumen is greater.

Fig. 12 shows the plate number predicted for a liquid-cooled, 100 cm long, 400
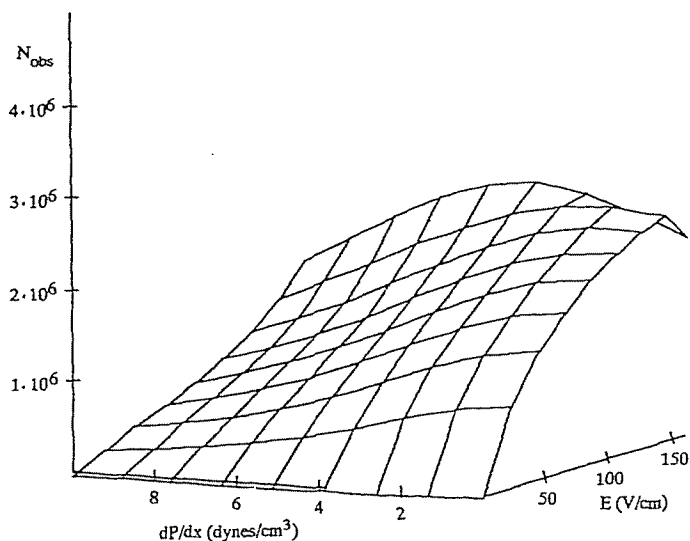

Fig. 13. Observed plate number for an air cooled 100 cm long, 100 × 200 μm capillary assuming a 2-mm long sample. Performance is severely degraded in comparison with Fig. 8. There is little benefit in applying a pressure gradient.
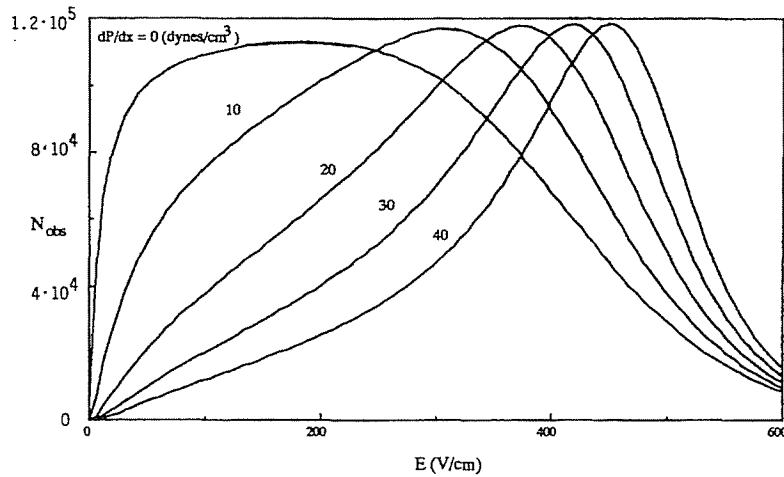
A 29

THERMAL MODEL OF CE   207

Fig. 14. Observed plate numbers predicted for a liquid cooled, 20 cm long, 100 × 200 μm capillary, assuming a 2-mm long initial sample size. The sample size greatly degrades performance.

× 530 μm capillary. This large bore capillary can reach high plate numbers with the assistance of a pressure gradient.

    For comparison, Figs. 13–15 show plate numbers predicted for these capillaries assuming an initial sample length of 2 mm. Such a sample size severely limits the performance of all the columns. Performance is most drastically reduced in the 20 cm long 100 × 200 μm column because of its short length. In contrast, much less degradation occurs in the 100 cm long 400 × 530 μm column.
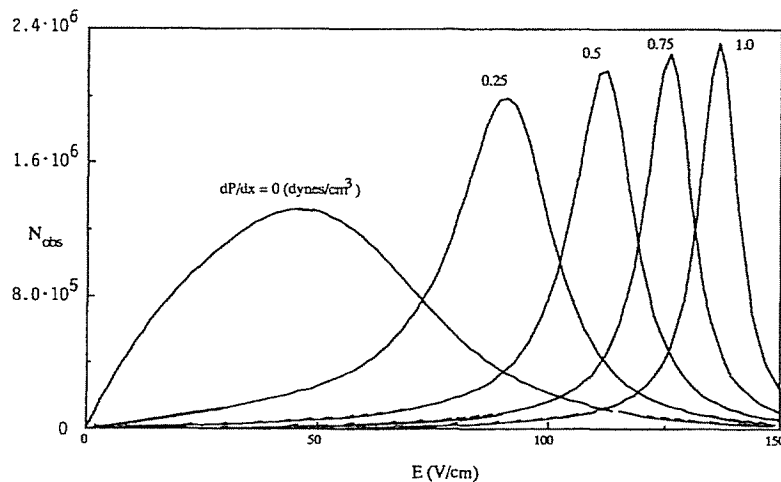

Fig. 15. Observed plate number predicted for a liquid cooled 100 cm long, 400 × 530 μm capillary, assuming a 2-mm long initial sample. Good performance can be obtained without a pressure gradient, and the plate number can be roughly doubled by applying a pressure gradient.

A 30

DISCUSSION

Thermal model

The results show that a constant-conductivity model can seriously underpredict the temperature in a capillary at high power levels. This can adversely affect estimates of electrophoretic mobility, residence time, and plate number.

The simulation incorporating a 1 cm/s draft points up the extreme sensitivity of air cooled capillaries to drafts. Air cooled capillaries function rather like hot-wire anemometers. It is important to keep them carefully shielded from air currents.

Forced liquid cooling offers substantially better heat transfer. Liquid cooled capillaries can be operated at significantly higher voltages than air cooled ones. The increase in voltage may be as much as a factor of 20; in practice however, the autothermal effect probably limits the increase to a factor less than 10. But since the autothermal effect amplifies electrophoretic mobility, the increase in migration velocities may yet be as much as 20 times.

It is possible that the two capillaries which exhibited superheating possess very smooth lumen surfaces which provide no nucleation sites. The lumens are too large to interfere with bubble formation through capillary pressure; they would have to have radii of about 0.1 μm to give the observed superheating. This conclusion is supported by the smallest capillary (Fig. 7), which exhibited no superheating.

Superheating has no obvious application in CE. However, carefully selected capillaries could provide convenient vessels for studying phenomena in aqueous solutions above the boiling point without the need for high-pressure apparatus.

Band spreading model

In cases where column performance is limited by thermal effects rather than sample loading or other dispersive phenomena, it is possible to improve the plate number to near the limit set by sample size and molecular diffusion by imposing a pressure gradient. The simulations show that at a particular pressure gradient, the optimal electric field is narrowly defined. This is because of the autothermal effect's strong non-linearity. The theoretical relations given here can only be used to provide an initial guess of the best conditions, owing to the non-linear variation of viscosity and of the mobility of buffer and sample ions.

Large capillaries appear to benefit the most from application of a pressure gradient. Such capillaries suffer greatly from thermal Taylor dispersion because their large radii preclude efficient radial diffusive averaging. But by flattening the velocity profile with a pressure gradient, plate numbers in excess of 10^6 can be obtained. Larger capillaries would ease detection difficulties since sample capacity increases with the diameter squared. Wall interactions also would become less deleterious.

The dispersion simulations illustrate the constraint on column performance imposed by the initial length of the sample. This constraint can be overcome, to some degree, by lengthening the column. For example, the upper limit on plate number based on sample size for a 100-cm column and 2-mm sample pulse is $3 \cdot 10^6$ plates. Samples this small may pose a detection problem. However, if one uses a large diameter capillary, sample loading can be increased even while sample length is decreased, *e.g.*, a 2-mm long sample in a 500-μm capillary contains 20 times more material than a 1-cm long sample in a 50-μm capillary.

CONCLUSIONS

The autothermal effect makes CE capillaries run significantly hotter than constant conductivity models predict. The autothermal model presented here is in substantial agreement with experimental measurements of capillary temperatures. The temperature simulations illustrate the sensitiviy of air cooled capillaries to drafts. Forced liquid cooled capillaries offer better temperature control and allow higher operating voltages.

The method we have proposed to reduce thermal band broadening, by imposing a small Poiseuille flow, appears promising. Best results should be obtained with capillaries which are considered too large to be useful for CE: It appears possible to obtain plate numbers in excess of 10^6 in capillaries as large or larger than 400 μm.

Performance of any CE column is limited by the initial length of the sample. Shorter samples improve plate number at the expense of detectability. Detectability can be maintained in large diameter capillaries, which offer the possibility of maintaining or increasing sample volume while decreasing sample length.

SYMBOLS

Bi_{OA}	overall Biot number, $h_{OA}R_L/k$
Bi_S	surface Biot number, $h_S R_P/k$
c_1	variation of concentration from mean value
c_p	heat capacity
D	diffusion coefficient
D_T	effective, or Taylor, diffusion coefficient
e	emissivity
E	electric field
$f(\lambda)$	autothermal function
g	gravitational acceleration
Gr	Grashof number, $D^3 \rho^2 \beta g \Delta T/\mu^2$
h_{OA}	overall heat transfer coefficient
h_S	surface heat transfer coefficient
J_0, J_1	Bessel functions
k	thermal conductivity of water
k_C	thermal conductivity of coolant
k_P	thermal conductivity of polyimide
k_W	thermal conductivity of capillary wall
L	length of capillary
m_2	second moment of concentration distribution
N, N_{obs}	plate number and observed plate number
Nu_C, Nu_R, Nu_S	convective, radiative and surface Nusselt numbers
P	pressure
Pr	Prandtl number, $c_P \mu/k$
r	radial coordinate
R_L	lumen radius
R_P	polyimide outer radius
R_W	silica wall outer radius

A 32

W. A. GOBIE, C. F. IVORY

t	time
T	temperature in lumen
T_C	coolant temperature
T_s	surface temperature
T_0	reference temperature for electrical conductivity
u	sample velocity
U	mean velocity
x	axial coordinate
z	initial length of sample
α, α'	electrophoretic and electroosmotic mobility
α_0, α'_0	reference electrophoretic and electroosmotic mobility
α_1, α'_1	electrophoretic and electroosmotic mobility temperature coefficients
β	coefficient of thermal expansion
ΔT_{ref}	characteristic temperature rise
η	dimensionless radial coordinate, r/R_L
η'	variable of integration
κ	electrical conductivity
κ_0	reference electrical conductivity
κ_1	electrical conductivity temperature coefficient
λ	autothermal parameter
μ	viscosity
μ_0	reference reciprocal viscosity
μ_1	temperature coefficient of reciprocal viscosity
χ	departure from mean velocity
ρ	density
σ	Stephan–Boltzmann constant
θ	dimensionless temperature
ω	characteristic dimensionless variation of reciprocal viscosity

REFERENCES

1 J. W. Jorgenson and K. D. Lukacs, *Science (Washington, D.C.)*, 222 (1983) 266.
2 G. I. Taylor, *Proc. Roy. Soc.*, A219 (1953) 186.
3 E. Grushka, R. M. McCormick and J. J. Kirkland, *Anal. Chem.*, 61 (1989) 241.
4 E. Lynch and D. A. Saville, *Chem. Eng. Commun.*, 9 (1981) 201.
5 A. E. Jones and E. Grushka, *J. Chromatogr.*, 466 (1989) 219.
6 S. Hertén, *Chromatogr. Rev.*, 9 (1967) 122.
7 R. B. Bird, W. E. Stewart and E. N. Lightfoot, *Transport Phenomena*, Wiley, New York, 1960.
8 J. O. N. Hinkley, *J. Chromatogr.*, 109 (1975) 218.
9 M. Coxon and M. J. Binder, *J. Chromatogr.*, 101 (1974) 1.
10 W. H. McAdams, *Heat Transmission*, McGraw-Hill, New York, 3rd ed., 1954, p. 176.
11 W. N. Gill and R. Sankarasubramanian, *Proc. R. Soc. London, Ser. A*, 316 (1970) 341.
12 R. Aris, *Proc. R. Soc. London, Ser. A*, 235 (1956) 67.
13 R. C. Reid, J. M. Prausnitz and T. K. Sherwook, *The Properties of Gases and Liquids*, McGraw-Hill, New York, 3rd ed., 1977, p. 454.

A 33

TAB 4

CHROM. 21 311

NATURE OF TEMPERATURE GRADIENTS IN CAPILLARY ZONE ELECTROPHORESIS

ALLAN E. JONES

Engineering Department, E.I. du Pont de Nemours, Wilmington, DE 19898 (U.S.A.)

and

ELI GRUSHKA*,ᵃ

Central Research and Development, E.I. du Pont de Nemours, Wilmington, DE 19898 (U.S.A.)

(Received September 5th, 1988)

SUMMARY

An expression for the radial temperature profile in capillary zone electrophoresis was derived, taking into account the temperature dependence of the buffer electrical conductivity and the polyimide coating of the quartz capillary. Calculations show that in typical capillary zone electrophoresis experiments; *i.e.*, capillaries with 50–100 μm I.D., 375 μm O.D., and up to 5 W power input, the temperature profile rigorously derived is nearly identical to a parabolic profile. At high input powers, the parabolic approximation underestimates the temperature at the capillary center.

INTRODUCTION

Capillary zone electrophoresis (CZE) is a separation technique the plate height efficiency of which can be very high. In practice, however, the theoretically calculated efficiencies are not observed. One possible reason for the lower than theoretical efficiencies can be traced to heating effect due to the passage of current through the capillary[1]. This heating effect causes a temperature difference between the center of the capillary and the wall, which, in turn, causes differences in the viscosity of the buffer electrolyte within the column. The resulting radial viscosity gradient produces a velocity difference between the center of the capillary and the wall. This velocity difference gives rise to mass transfer effects which lower the system efficiency. Grushka *et al.*[2] have studied the effect of temperature differences on the efficiency of CZE. In that study the assumed temperature profile produced a parabolic velocity profile across the capillary. In the present communication, this parabolic temperature profile assumption is justified.

ᵃ Permanent address: Department of Inorganic and Analytical Chemistry, The Hebrew University, Jerusalem, Israel.

THEORY

Derivation of temperature profile

Modern CZE separations are carried out in quartz capillaries that are coated with a thin layer of polyimide. In this analysis, R_1 symbolizes the internal radius, R_2 the quartz radius and R_c the total radius of the capillary. The temperature dependence of the thermal and electrical conductivities should be taken into account in the heat balance equations in order to obtain the correct temperature profile. Using an approach similar to that of Coxon and Binder[3] and by Brown and Hinckle[4], the heat balance equation for CZE can be written as

$$\frac{1}{r}\frac{d}{dr}\left(r\frac{dT}{dr}\right) = -\frac{G}{k_1} \tag{1}$$

where T is the temperature, r is the radial position, G is the heat generation per unit volume and k_1 is the termal conductivity of the buffer solution. The boundary condition is

$$-R_1 k_1 \frac{dT}{dr} = U R_1 (T_1 - T_s) \qquad \text{at } r = R_1$$

where R_1 is the internal radius of the capillary, T_1 and T_s are the temperature at the glass wall and the capillary surroundings (*i.e.*, a thermostated bath) respectively, (at R_1), and k_1 is the thermal conductivity of the buffer. The quantity UR_1 is related to the heat dissipation through the capillary wall, and it is given by

$$\frac{1}{R_1 U} = \frac{1}{k_2}\ln\left(\frac{R_2}{R_1}\right) + \frac{1}{k_c}\ln\left(\frac{R_c}{R_2}\right) + \frac{1}{R_c h} \tag{2}$$

where R and k indicate radius and thermal conductivity and subscripts 2 and c indicate quantities relating to the quartz glass and polyimide coating, respectively. Because of the electrical conductivity dependence on temperature, the rate of heat generation will be written as

$$G = G_0\left[1 + \alpha\left(\frac{T - T_s}{T_s}\right)\right] \tag{3}$$

where α is the temperature coefficient of electrical conductivity of the buffer, G_0 is the rate of heat generation in the absence of temperature dependence of the electrical conductivity and T_s is the temperature of the capillary surroundings. When this temperature dependence of the heat generation is taken into account, the equation describing the heat balance can be written as[3]

$$\frac{1}{y}\frac{\partial}{\partial y}\left(y\frac{\partial\theta}{\partial y}\right) = -S(1 + \alpha\theta) \tag{4}$$

A 35

TEMPERATURE GRADIENTS IN CZE   221

where

$$y = \frac{r}{R_c}$$

$$S = \frac{G_0 R_c^2}{k_1 T_s}$$

$$\theta = \frac{T - T_s}{T_s}$$

The boundary condition is

$$-k_1 \frac{d\theta}{dy} = U R_c \theta_1 \qquad \text{at } y = y_1$$

The solution of eqn. 4 is

$$\theta = A J_0(\beta y) - \frac{1}{\alpha} \tag{5}$$

where $\beta^2 = \alpha S$ and A is a constant of integration. Using the boundary conditions it can be shown that

$$A = \frac{1}{\alpha[J_0(\beta y_1) - (\beta/\gamma) J_1(\beta y_1)]} \tag{6}$$

where

$$\gamma = \frac{U R_c}{k_1}$$

The expression for the temperature profile is, therefore:

$$\theta = \frac{1}{\alpha} \left\{ \frac{J_0(\beta y)}{[J_0(\beta y_1) - (\beta/\gamma) J_1(\beta y_1)]} - 1 \right\} \tag{7}$$

or

$$T = \frac{T_s}{\alpha} \left\{ \frac{J_0(\beta y)}{[J_0(\beta y_1) - (\beta/\gamma) J_1(\beta y_1)]} - 1 \right\} + T_s \tag{8}$$

Evaluation of the temperature profile

The temperature expression in eqn. 8 is similar to the expression obtained by Coxon and Binder[3]. However, eqn. 8 accounts for the fact that the quartz capillary tubing used in CZE is coated with polyimide. To evaluate the temperature profile, it is

A 36

essential to obtain G_0, which is needed to calculate β. Coxon and Binder[3] did not describe the manner by which G_0 is obtained. Since the correct evaluation of G_0 is crucial to the proper determination of the temperature, we will elaborate here on this point.

Since heat dissipation in the capillary is from the center to the wall, we will re-write the expression for G in terms of a differential equation in the radial direction

$$dG = 2\pi r L G_0 (1 + \alpha\theta) dr$$

Or, in terms of reduced radius

$$dG = 2\pi L R_c^2 G_0 (1 + \alpha\theta) y \, dy \tag{9}$$

Substituting for θ from eqn. 7 and rearranging, we get

$$dG = 2\pi L R_c^2 G_0 [\alpha A J_0(\beta y)] y \, dy \tag{10}$$

Since the electrical conductivity of the buffer varies radially with the temperature, we integrate over y. Thus, a substitution for A and integration between 0 and y_1 yield

$$G = \frac{2\pi L R_c^2 G_0 y_1 J_1(\beta y_1)}{\beta[J_0(\beta y_1) - (\beta/\gamma) J_1(\beta y_1)]} \tag{11}$$

Eqn. 11 allows us to obtain the value of G_0 by iteration (note that β is also a function of G_0). However, due to the transcendental nature of eqn. 11, numerical procedures must be used.

Calculations

A computer program was written to compute G_0 iteratively for a given input power. The iteration of eqn. 11 should be done with caution since the equation can have many roots. The only physically significant solution is the smallest root. Therefore, the iteration should start with a low initial estimate of G_0 to insure the proper convergence.

Once the value of G_0 is determined, the temperature profile is calculated using eqn. 8, as well as the following parabolic profile

$$T = T_s + \frac{G R_c}{2U} + \frac{G R_1^2}{4k_1}\left(1 - \frac{r^2}{R_1^2}\right) \tag{12}$$

The values of the various parameters used in the calculation are given in the sub-titles of Tables I and II. The radii of the capillary used in the calculations are typical of the sizes used in practice; *i.e.*, inner diameter of 50 μm, quartz capillary outer diameter of 345 μm and polyimide coating thickness of 15 μm (giving a total outside diameter of 375 μm). Assuming that an 1-degree change will cause a 2% change in the conductivity, the value of α is then 7.75.

Table I gives the temperature at the capillary center, at the inner wall and ΔT as